Axisymmetric pulse recycling and motion in bulk semiconductors

L. L. Bonilla and R. Escobedo
Universidad Carlos III de Madrid, Escuela Politécnica Superior, 28911 Leganés, Spain

F. J. Higuera
ETS Ingenieros Aeronáuticos, Plaza Cardenal Cisneros 3, 28040 Madrid, Spain

(Received 18 July 2001; published 19 December 2001)

The Kroemer model for the Gunn effect in a circular geometry (Corbino disks) has been numerically solved. The results have been interpreted by means of asymptotic calculations. Above a certain onset dc voltage bias, axisymmetric pulses of the electric field are periodically shed by an inner circular cathode. These pulses decay as they move towards the outer anode, which they may not reach. As a pulse advances, the external current increases continuously until a new pulse is generated. Then the current abruptly decreases, in agreement with existing experimental results. Depending on the bias, more complex patterns with multiple pulse shedding are possible.

DOI: 10.1103/PhysRevE.65.016607 PACS number(s): 05.45.−a, 47.54.+r, 73.50.Fq, 82.40.Bj

I. INTRODUCTION

Propagation of pulses naturally occur in excitable media, which exhibit a large response when a sufficiently strong perturbation disturbs the only stable stationary homogeneous state [1]. Examples are the propagation of an action potential along the axon of a nerve [2], propagation of a grass fire on a prairie, pulse propagation through cardiac cells [2], reaction diffusion [3], or ecological systems [1]. While a vast literature is devoted to the mathematical description of pulses propagating in unbounded media, less is known about pulse generation from boundaries and propagation in finite domains, particularly in multidimensional domains.

That boundaries and boundary conditions play an important role in pulse creation and annihilation is well understood in the context of semiconductor instabilities [4]. Device geometry and bias conditions are crucial for instabilities and related nonlinear dynamics to appear. Nice examples can be found in the experiments by Willing and Maan on repeated pulse propagation in semi-insulating GaAs [5]. They considered rectangular samples with two attached parallel planar contacts or with point contacts at different dc voltage. In the first situation, planar pulses were periodically generated at the cathode and moved towards the anode where they disappeared. This phenomenon is analogous to the well-known Gunn effect in bulk *n*-GaAs [6]. In the case of point contacts, circular waves were repeatedly generated at the cathode, and vanished before arriving at the anode [5]. Theoretical studies of self-sustained oscillations in semi-insulating GaAs are scarce even in one-dimensional geometries (cf. Ref. [7] and references cited therein). However, the observed phenomena can be qualitatively understood within the simpler Kroemer model for the Gunn effect in bulk *n*-GaAs [8]. An asymptotic study of this model on a one-dimensional spatial support can be used to understand pulse propagation in samples with planar contacts [9]. A simple study of pulse propagation in samples with point contacts could consist of analyzing the Kroemer model in a axisymmetric sample: a circular sample of bulk *n*-GaAs with a point contact (cathode) at its center and an attached concentric circular outer contact (anode). This configuration is known as *Corbino geometry* [4]. In this paper, we carry out a numerical study of pulse dynamics in the Kroemer model with Corbino geometry. Depending on the dc voltage bias and contact resistivity, we observe stationary field and current and self-sustained oscillations (periodic or not) due to pulse propagation and recycling. Pulses may or may not arrive at the anode before a new pulse is generated at the cathode. These results are presented in Sec. III after a short description of the Kroemer model in Corbino geometry given in Sec. II. The numerical results are interpreted by means of an asymptotic analysis in Sec. IV. Section V contains our conclusions and the numerical method we use is described in the Appendix.

II. EQUATIONS AND BOUNDARY CONDITIONS

The Kroemer model consists of the following equations and boundary conditions (in dimensionless units) for the concentration of free carriers (electrons) n and the electric potential φ:

$$\frac{\partial n}{\partial t}+\vec{\nabla}\cdot(n\vec{v}-\delta\vec{\nabla}n)=0, \tag{1}$$

$$\nabla^2\varphi=n-1, \tag{2}$$

$$\vec{v}(\vec{E})=\vec{E}\frac{1+v_sE^3}{1+E^4}, \tag{3}$$

$$\vec{x}\in\Sigma_c:\ \vec{E}\cdot\vec{N}=\rho(n\vec{v}-\delta\vec{\nabla}n)\cdot\vec{N}\quad\text{and}\quad\varphi=0, \tag{4}$$

$$\vec{x}\in\Sigma_a:\ \vec{E}\cdot\vec{N}=\rho(n\vec{v}-\delta\vec{\nabla}n)\cdot\vec{N}\quad\text{and}\quad\varphi=\Phi. \tag{5}$$

Here Eqs. (1) and (2) are the charge continuity and Poisson equations, respectively. The dimensionless electric field is $\vec{E}=\vec{\nabla}\varphi$ and $E=|\vec{E}|$. In these equations, the electron density has been scaled with the uniform concentration of donor impurities in the semiconductor, $N_D=10^{15}$ cm^{-3}, and the electric field with the field characterizing the intervalley transfer

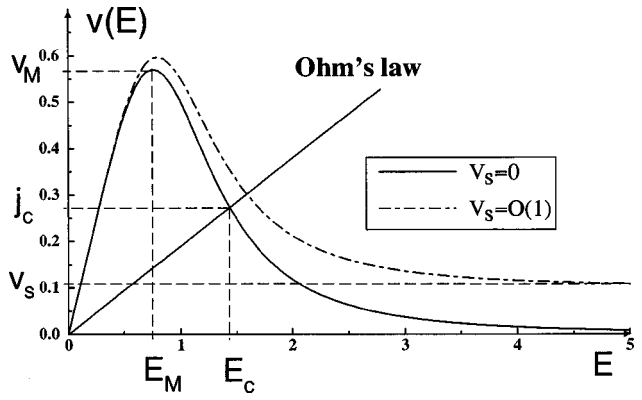

FIG. 1. Drift velocities and Ohm's law. $v(E)=|\vec{v}(\vec{E})|$ has a maximum $v_M=3^{3/4}/4$ at $E=E_M=1/3^{1/4}$ (for $v_s=0$), followed by a region of negative differential mobility for $E>E_M$. At large fields $E\gg 1$, the electron velocity monotonically decreases to a value v_s, which may be zero.

responsible for the negative differential mobility involved in the Gunn oscillation, $E_R=3.1$ kV/cm. Distances and times have been measured with the dielectric length and the dielectric relaxation time, $l_1=\epsilon E_R/(eN_D)\approx 0.276$ μm and $l_1/(\mu_0 E_R)\approx 1.02$ ps, respectively (μ_0 is the zero-field electron mobility; see, e.g., [10] for details). The unit of electric potential is $E_R l_1\approx 0.011$ V. The carrier drift velocity of Eq. (3), $\vec{v}(\vec{E})$, is already written in dimensionless units, and it has been depicted in Fig. 1. We assume that the diffusion coefficient is constant, $\delta\approx 0.013$ (at 20 K).

Boundary and bias conditions need to be imposed at the interfaces between semiconductor and contacts, $\Sigma_{c,a}$. Our boundary conditions (4) and (5) assume that the normal components of the electron current density and the electric field are proportional at the semiconductor–contact boundary (Ohm's law) [10], (in these equations, $\vec{N}$ is the unit normal to $\Sigma_{c,a}$ directed towards the semiconductor). For simplicity, we choose all contact resistivities ρ to be equal. Bias conditions are chosen to be $\varphi=0$ at the cathode Σ_c (injecting contact) and $\varphi=\Phi$ (the applied voltage) at the anode Σ_a (receiving contact). Typically $\delta>0$ is very small, so that diffusion matters only inside boundary layers near the contacts or inside thin shock waves [10,9]. The latter are charge accumulations that will be treated simply as discontinuities of the electric field [9,10]. Thus diffusion effects may be left out of the conservation equation (1) when interpreting the results. If we set $\delta=0$, the first boundary condition in Eq. (5) should be omitted.

We can write an Ampère's equation for the total current density (electronic plus displacement), $\vec{j}$, by eliminating n from Eq. (1) using Eq. (2)

$$\vec{\nabla}\cdot\vec{j}=0,$$

with

$$\vec{j}=(1+\nabla^2\varphi)\vec{v}-\delta\vec{\nabla}(\nabla^2\varphi)+\frac{\partial\vec{E}}{\partial t}. \tag{6}$$

In the Corbino geometry considered in this paper, this equation can be simplified further. Let r_c and $r_a>r_c$ be the radii of cathode and anode, respectively. The electric field and current density are now directed along the radial direction $\vec{E}=E(r,t)\vec{r}/r$, $E(r,t)=\partial\varphi(r,t)/\partial r$, and $\vec{j}=J(t)\vec{r}/r^2$, so that Eq. (6) becomes

$$\frac{\partial E}{\partial t}+v(E)\left[1+\frac{1}{r}\frac{\partial(rE)}{\partial r}\right]-\delta\frac{\partial}{\partial r}\left[\frac{1}{r}\frac{\partial(rE)}{\partial r}\right]=\frac{J}{r}, \tag{7}$$

where $2\pi J(t)$ is the current through the external circuit, $i(t)=\int_{\Sigma_c}\vec{j}\cdot\vec{N}dA=2\pi J(t)$. Equation (7) for $E(r,t)$ and $J(t)$ should be solved with the following bias and boundary conditions

$$\frac{1}{L}\int_{r_c}^{r_a}E\,dr=\phi, \tag{8}$$

$$E=\rho\left(\frac{J}{r}-\frac{\partial E}{\partial t}\right)\quad \text{at } r=r_c,r_a, \tag{9}$$

where $L\equiv r_a-r_c$ and $\phi=\Phi/L$.

It is known (see, e.g., [10]) that planar dipole waves may appear in long samples when $\rho>4/3$, for which the straight line $j=E/\rho$ representing Ohm's law intersects the drift velocity curve $j=v(E)$ at a point (E_c,j_c) on the second branch of this curve, as sketched in Fig. 1. (In particular, $E_c\approx\rho^{1/4}$ and $j_c\approx\rho^{-3/4}$ for large ρ.) This is the case we will consider in the present paper.

III. NUMERICAL RESULTS

We have solved numerically Eqs. (7) and (8) together with the boundary conditions (9) at $r=r_c$ and $r=r_a$. Appropriate initial conditions were given for $E(r,0)$. Parameter values were $\rho=2$, $\delta=0.013$, $r_c=10$ and $r_a=50$ and 90 (i.e., $L=40$ and 80 resp.). The bias ϕ was used as a control parameter for two different electron velocity curves $v_s=0$ and $v_s=0.1$, representing zero and nonzero saturation velocities at high electric fields. These parameter values are appropriate for *n*-GaAs and are consistent with previous studies [10]. Consider first the characteristic current-voltage curve $J(\phi)$ of Fig. 2. There we can mark three different regimes, already present in experiments [5].

Regime I. $0<\phi<\phi_\alpha\approx 0.168$. Stable solutions are stationary and $J(\phi)$ is well approximated by a straight line with slope ≈ 31.5.

Regime II. $\phi_\alpha<\phi<3\phi_\alpha/2\approx 0.25$. Above the onset bias for current oscillations, there are small-amplitude (10–20 % of the overall current signal) sinusoidal current self-oscillations. The oscillation maxima and minima are about $J_c\approx 5.4$ and $J_{min}\approx 4$, respectively. The electric field profile is a triangular pulse, which is recycled at the cathode, it advances and soon disappears at $r\approx 25$ (quenched-mode oscillation). See Fig. 3.

Regime III. $3\phi_\alpha/2<\phi<\phi_\omega$. The upper critical bias ϕ_ω is finite for $v_s>0$ (e.g., $\phi_\omega\approx 15$ if $v_s=0.1$) and infinite for $v_s=0$. There are large-amplitude (60% of the overall current

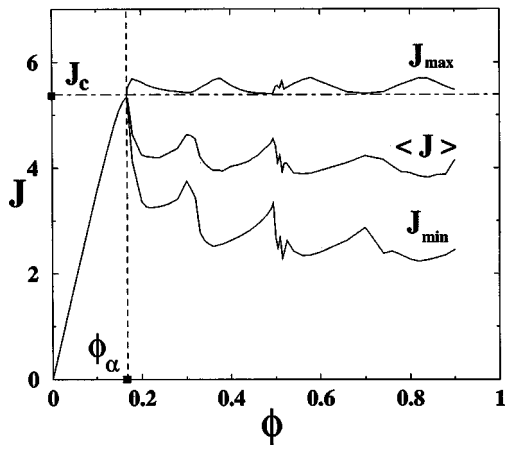

FIG. 2. Current-voltage characteristic curve $J(\phi)$ for $v_s=0$. If $0<\phi<\phi_\alpha$, the stable electric field profile is stationary. For $\phi>\phi_\alpha$, we have depicted the maxima, minima, and time-averaged values of the current self-oscillations. There are small-amplitude current self-oscillations if $\phi_\alpha<\phi<2\phi_\alpha/3$, and large-amplitude self-oscillations due to pulse recycling and motion if $2\phi_\alpha/3<\phi<\phi_\omega$). ϕ_ω is finite for $v_s>0$ and infinite for $v_s=0$.

signal) current self-oscillations. These oscillations are mostly time periodic, although there are narrow bias intervals of aperiodic oscillations. Their maxima $J_{max}(\phi)$ are always close to J_c, while their minima $J_{min}(\phi)$ take values on a wider range of currents. Electric field profiles consist of moving triangular pulses. For $\phi>\phi_\omega$, the stable field profile is again stationary as shown in Fig. 4. These results qualitatively agree with the experimental observations of self-sustained oscillations in semi-insulating GaAs reported in Ref. [5]. The experimental samples were rectangular and contained two well-separated point contacts. It was observed that self-oscillations of the current were due to circular dipole waves that were recycled at the cathode, expanded towards the anode, and vanished without ever reaching it. The current signal was similar to that in Fig. 5 below. Semi-insulating GaAs is described by model equations different from the Kroemer model. However, qualitative agreement of experimental data with our results for the axisymmetric Kroemer model suggest that a theoretical interpretation of self-oscillations similar to that in Sec. IV could also be appropriate for semi-insulating GaAs.

We shall now describe the more interesting self-

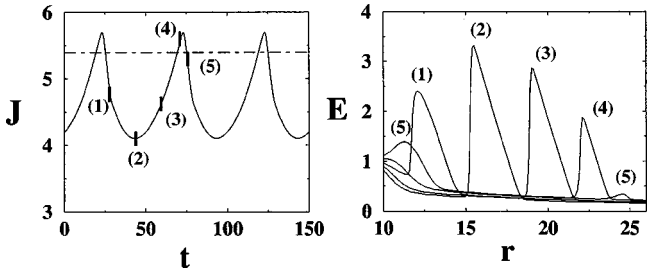

FIG. 3. Total current density (left) and electric field profiles (right) for $\phi=0.18$. The electric field profiles are depicted at the times marked on the graph of $J(t)$. The horizontal line in the latter corresponds to the value J_c.

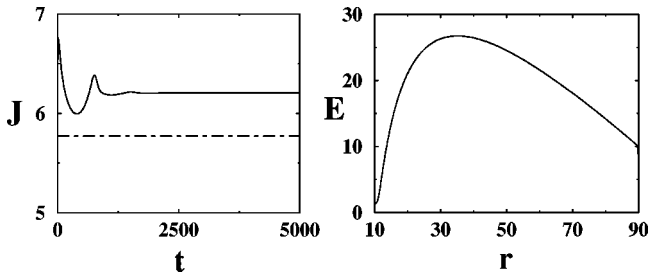

FIG. 4. Stationary solution for $\phi=20$, $L=80$, and $v_s=0.1$. J evolves towards $J\approx6.2$ greater than $J_c=5.77$. The maximum electric field $E_+\approx26.75$ is reached at $R_b\approx35.12$. Field values at the boundaries are $E(r_c)=1.25$ and $E(r_a)=0.14$.

oscillations in regime III, starting with a bias interval of time-periodic oscillations. Stationary solutions and their stability properties will be described elsewhere.

A. Time-periodic oscillations for $0.35<\phi<0.5$ and $v_s=0$

Figure 5 shows one period of $J(t)$ for different bias values in this interval. The electric field profile $E(r,t)$ consists of a single triangular pulse traveling towards the anode when $J(t)$ is increasing. When $J(t)$ decreases, one triangular pulse disappears and a new one appears at the cathode. The gradual increase of the current when there is only one pulse in the sample lasts longer than the drop to low current values. Notice that the current drop lasts the same for all bias values, while the stage of current growth increases with ϕ.

This situation is remarkably different from that for the one-dimensional geometry corresponding to parallel planar contacts: the current signal is flat when there is only a single pulse far from the contacts and the stages of the current increase and drop are very short [10]. Other noticeable features in Fig. 5 are (i) a new wave is nucleated as J surpasses a critical value J_c (bias independent); (ii) the current overshoot above J_c decreases as ϕ increases, and (iii) there is a second local maximum of the current, and the width of the region between the two local maxima increases with ϕ. Let us explain in more detail the field profiles corresponding to

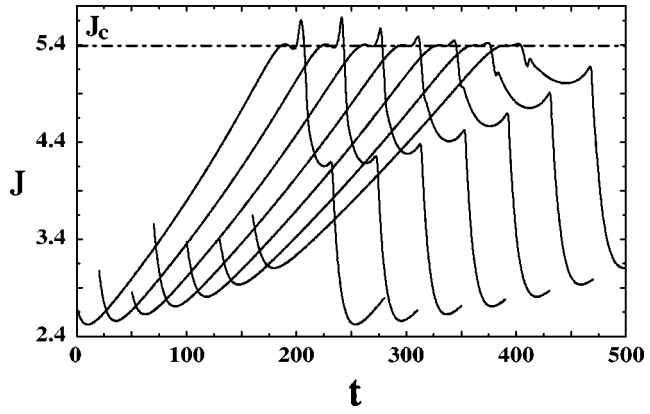

FIG. 5. Current vs time during one period of the self-oscillations for $\phi\in(0.35,0.5)$. Values of ϕ are 0.36, 0.38, 0.4, 0.42, 0.44, 0.46, and 0.48, depicted from left to right, and the critical current at which a new wave is nucleated is $J_c=5.39$.

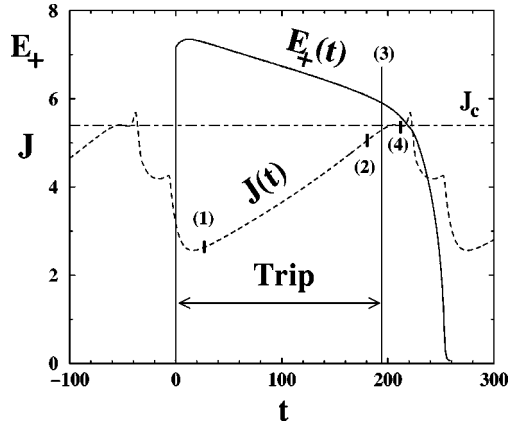

FIG. 6. Evolution of $J(t)$ and $E_+(t)$ during one oscillation period for $\phi=0.38$ and $v_s=0$, during the time interval $0<t<\Delta t \approx 200$, where there is a single pulse in the sample. Marked times are (1) 30, (2) 180, (3) 195, and (4) 215.

these stages of the self-oscillation.

Figures 6 and 7 show details of the current signal during one period of the self-oscillation for $\phi=0.38$ and $v_s=0$. Also shown are the maxima of the electric field for the different pulses that appear in this time interval. From $t=0$ to $t=195$, there is a single pulse moving towards r_a. This wave is roughly a straight triangle of height and width $E_+(t)$, which is the maximum of the field inside the wave at time t. The back of the pulse can be approximated by a shock wave located at $R_b(t)$. As we describe below, self-oscillations in the bias interval considered here involve creation of new pulses and transient field disturbances at the cathode. In Fig. 7, $R_b'(t)$ and $R_b^{dis}(t)$ are the locations of the maximum field

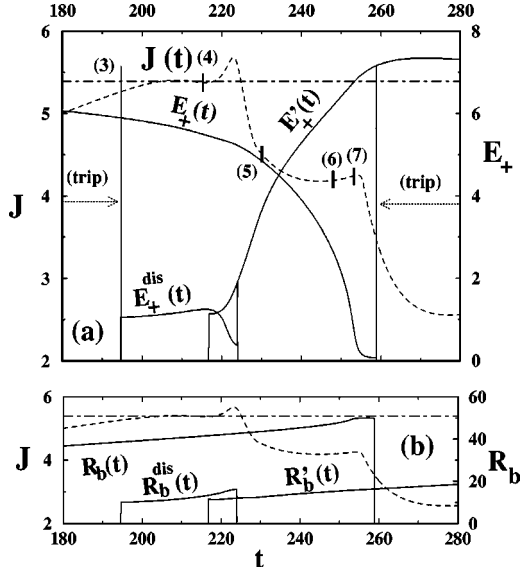

FIG. 7. Evolution of $J(t)$ and $E_+(t)$ during one oscillation period for $\phi=0.38$ and $v_s=0$. (a) Stage in which there are multiple pulses. (b) $R_b(t)$ during the multipulse stage. $R_b^{dis}(t)$ and $R_b'(t)$ are the locations of the maximum fields of the transient field disturbance and the new pulse, respectively. Marked times are (3) 195, (4) 215, (5) 230, (6) 248, and (7) 253.

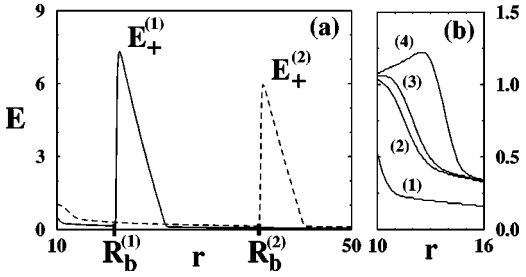

FIG. 8. (a) Electric field profile during the single-pulse stage at times (1) and (2) of Fig. 6. (b) Details of the field profile near the cathode: the slope at r_c increases with J; $dE(r_c)/dr=0$ for $J=J_c \approx 5.24$ at time (3).

of a new pulse and a transient pulselike field disturbance (both shed at the cathode), respectively. Figure 8(a) shows the electric field profile at the times marked (1) and (2) in Fig. 6. Figure 9(a) depicts the electric field near the cathode. A new pulse is shed from the cathode when J surpasses the critical value J_c at time (4) in Fig. 6. Between times (3) and (4) (with $J<J_c$), a field disturbance is shed from the cathode and it shrinks rapidly as it advances. Eventually as the first pulse disappears (slightly after the time corresponding to the second local maximum of the current), the new pulse shed at time (4) remains the only one in the sample. A new oscillation period starts then. Figure 9 shows details of the field profiles when there are more than one pulses in the sample.

B. Aperiodic current self-oscillations

For biases $\phi \geqslant 0.5$, periodic self-oscillations of the current alternate with voltage ranges of aperiodic oscillations. Figure 10 shows that the corresponding current signals may be rather complex, with several maxima and current overshoots above J_c.

Typically several pulses are present during different time intervals of the self-oscillation. The leftmost pulse may shrink as the second pulse increases, or it may reach it and

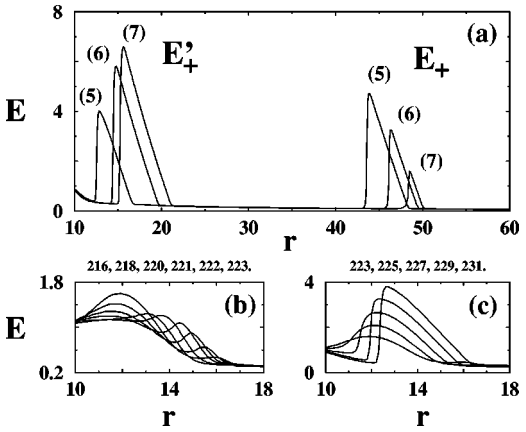

FIG. 9. (a) Electric field profiles during the multipulse stage at times marked as (5), (6), and (7) in Fig. 6 for $\phi=0.38$ and $v_s=0$. (b) Details of the unsuccessful attempt at shedding one pulse from the cathode for $J<J_c$. (c) Successful nucleation of the new pulse after time (4).

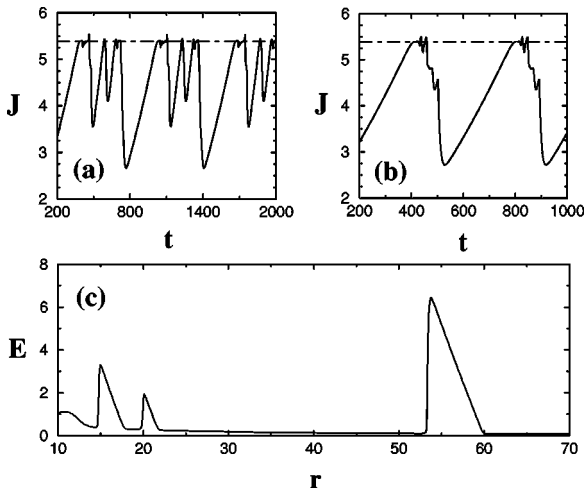

FIG. 10. (a) Complex current signal $J(t)$ for $\phi=0.5$ and a time interval $\Delta t\approx 650$. (b) Same for $\phi=0.52$ and $\Delta t\approx 400$. (c) Three-pulse electric field profile for $\phi=0.52$ and $\Delta t\approx 400$. In all cases, $v_s=0$. In (a) and (b), the horizontal line marks the critical current J_c.

coalesce with that pulse. Meanwhile the rightmost pulse may shrink or reach the anode. Pulses may be shed from the cathode or may nucleate inside the sample. The resulting current signals may even be apparently chaotic. A detailed study of all cases that are possible depending on the bias, will not be attempted here. Figure 11 depicts the local maxima of the current as a function of bias. A loss of periodicity at narrow bias intervals is apparent.

Comparing the case $v_s>0$ to that with $v_s=0$, we observe that the pulses move faster, the oscillations have smaller amplitudes and it is easier for several pulses to coexist when $v_s>0$. This may result in more complex shapes of the current signal, as shown in Fig. 12. The current signal is periodic in Figs. 12(a) and 12(b), although the period is longer in the latter due to separated current bursts. The current signal in Fig. 12(c) is aperiodic.

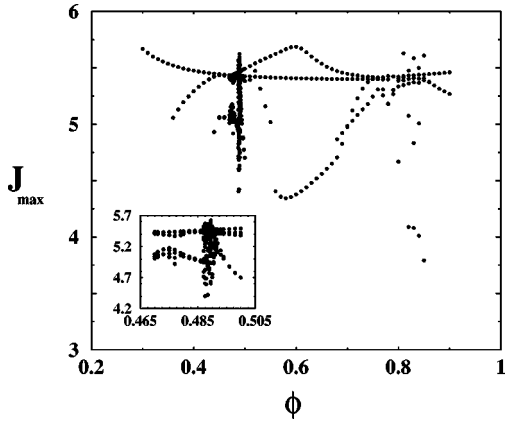

FIG. 11. Poincaré diagram depicting current maxima vs bias illustrating loss of periodic oscillations in narrow bias intervals. Parameters are $r_c=10$, $r_a=50$, and $v_s=0$.

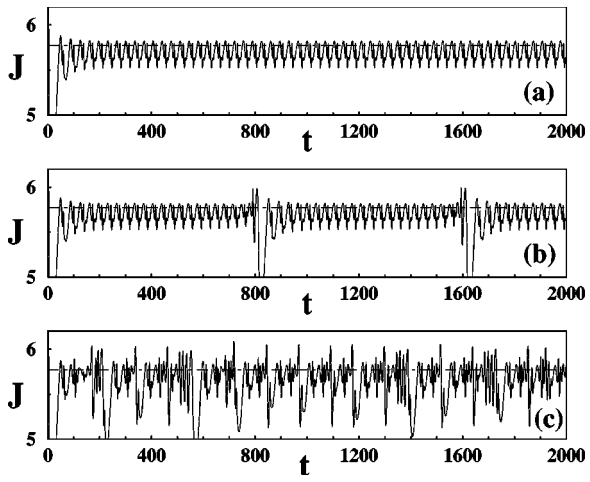

FIG. 12. Complex current signals for $v_s=0.1$, $r_c=10$, $r_a=50$ and several bias values: (a) $\phi=0.41$ (periodic signal), (b) $\phi=0.411$ (periodic signal with a longer period due to current bursts), and (c) $\phi=0.42$ (aperiodic signal). In all cases, $J(t)$ oscillates about $J_c=5.77$ with an approximate amplitude of 0.5.

IV. INTERPRETATION OF THE NUMERICAL RESULTS

In order to understand the shape of $J(t)$ in the time periodic regime and the fact that the pulses may vanish before reaching the anode, we present in this section a qualitative description of the asymptotic oscillatory solution for $r_a\gg r_c\gg 1$. In this case there is a wide range of voltages for which the pulses are detached from the contacts during most of their evolution time. A full analysis of the pulse dynamics should include descriptions of the evolution of a pulse far from the contacts and of the generation of new pulses at the injecting contact. The latter process is essentially as for the planar case [10] when $r_c\gg 1$, because the effect of the geometrical divergence is then negligible around the cathode. Analysis shows that, roughly, a pulse is shed when the current increases to $J=J_c\approx j_c r_c$, and then the current decreases while the new pulse grows and separates from the cathode. These results are in line with the numerical simulations of the preceding section.

In the remainder of this section we focus on the evolution of a pulse detached from the cathode. As in the planar case, such a pulse is a straight triangle made of a trailing edge which is a shock and a leading ramp which is a region depleted of electrons [10].

Consider first the region outside of the pulse. Time and space derivatives can be neglected in Eq. (7) for this region, which covers most of the sample, leading to the appoximate solution $v(E)=J/r$, which implies $E(r,t)=E_1(J/r)$, where $E_1(j)<E_2(j)$ are the two solutions of $v(E)=j$ for $v_s<j<v_M$. If $J\ll r$, the first branch of $v(E)$ is linear, and we have $E(r,t)\approx J/r$. The area under this stationary field profile is $\Phi_{out}=\int_{r_c}^{r_a}E_1(J/r)dr\approx J\ln(r_a/r_c)$.

The speed of trailing edge of the pulse, at $r=R_b(t)$, is given by the equal area rule for a shock raising the field from E_- to E_+; i.e., $V(E_+,E_-)\equiv\int_{E_-}^{E_+}v(E)dE/(E_+-E_-)$. For large pulses, $E_+\gg 1$ and the field immediately at the left of the shock is $E_-<E_M=O(1)$, so that we may approximate

$$V(E_+,E_-)=v_s+\frac{\int_{E_-}^{E_+}[v(E)-v_s]dE}{E_+-E_-}\sim v_s+\frac{C}{E_+} \quad (10)$$

with

$$C=\int_{E_1(v_s)}^{\infty}[v(E)-v_s]dE.$$

Here we have used that $V\sim v_s$ and $E_-\sim E_1(v_s)$ as $E_+\gg 1$. If $v_s=0$, then $C=\pi/4$ and $V(E_+,E_-)\sim\pi/(4E_+)$. In this case, the trailing front velocity is small, and small waves move faster than large ones. If $v_s>0$, then the waves move at a speed close to the saturation speed v_s.

The electron density at the leading ramp of the pulse is almost zero, so that the field obeys the Poisson equation $1+r^{-1}\partial(rE)/\partial r=n\approx 0$, whose solution is

$$E(r,t)=\frac{r_w^2(t)-r^2}{2r}\approx r_w-r \quad (11)$$

in the pulse. Here the constant of integration $r_w(t)$ is the intersection between the prolongation of the ramp and the r axis, and use has been made of the condition that the width of the pulse $W=r_w-R_b\approx E_+$ satisfies $r_w\gg W\gg 1$ to simplify the result. The area of the triangular pulse is $\Phi_{in}\approx E_+^2/2$, and, therefore, the bias condition (8) becomes

$$\Phi=\Phi_{in}+\Phi_{out}\sim\frac{E_+^2}{2}+J\ln\left(\frac{r_a}{r_c}\right). \quad (12)$$

The speed of the ramp, dr_w/dt, coincides with the speed of the electrons immediately ahead of the pulse

$$\frac{dr_w}{dt}=\frac{J}{r_w}. \quad (13)$$

This result can also be obtained by inserting Eq. (11) and $n=0$ into Eq. (7). Equations (12) and (13), along with

$$\frac{d(r_w-E_+)}{dt}=v_s+\frac{C}{E_+} \quad (14)$$

for the speed of the trailing shock (at $R_b\approx r_w-E_+$), suffice to determine the time evolution of J, r_w, and E_+ from a given initial state. Equation (14) can be rewritten as

$$\frac{dJ}{dt}=\frac{1}{\ln(r_a/r_c)}\left\{C-\left(\frac{J}{r_w}-v_s\right)\sqrt{2\left[\Phi-J\ln\left(\frac{r_a}{r_c}\right)\right]}\right\}, \quad (15)$$

where Eqs. (12) and (13) have been used.

The problem can be further simplified noticing that the speeds of the shock and the ramp are nearly equal to each other during most of the pulse lifetime,

$$v_s+\frac{C}{E_+}=\frac{J}{r_w}. \quad (16)$$

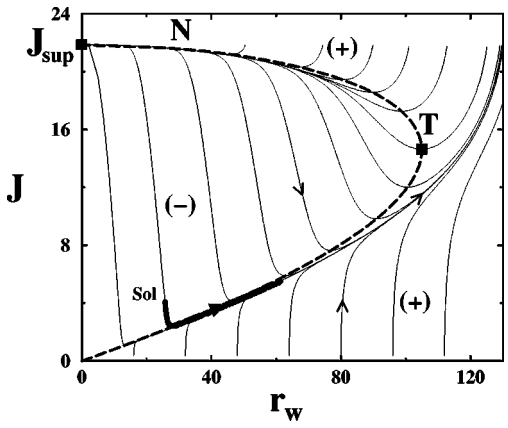

FIG. 13. Phase plane (r_w,J) showing the nullcline $dJ/dr_w=0$ (dash line) and the turning point for $v_s=0$ and a bias $\phi=0.6$. The thick line represents the trajectory of the solution for initial data $J(0)=4.1$ and $r_w=26$, until $J_c\approx 5.4$ is reached.

This occurs because the width of the pulse is small compared with the total distance it travels in the sample. Then a mismatch of the two speeds would lead either to the disappearance of the pulse or to its growth above the maximum size allowed by the bias in a time of order $E_+/\max(V,J/r_w)$. This time is short compared to the pulse lifetime. An algebraic relation between J and r_w can be obtained eliminating E_+ between Eqs. (12) and (16). This is plotted as a dashed curve in Fig. 13, which is the phase plane of Eqs. (13) and (15) for the case with $v_s=0$. As can be seen, the trajectories tend rapidly to the lower branch of the dashed curve and then rise along this branch obeying Eq. (13) until either: (i) r_w reaches its maximum possible value, corresponding to the turning point T, or (ii) J reaches the critical value J_c for nucleation of a new pulse, whichever happens first.

When $v_s=0$ the turning point is

$$J_T=\frac{2\Phi}{3\ln\left(\frac{r_a}{r_c}\right)},\quad r_{wT}=\frac{4}{\pi\ln\left(\frac{r_a}{r_c}\right)}\left(\frac{2\Phi}{3}\right)^{3/2}. \quad (17)$$

Then maximum radius of the pulse is either r_{wT} or

$$r_{wc}=\frac{4J_c}{\pi}\sqrt{2\left[\Phi-\ln\left(\frac{r_a}{r_c}\right)\right]}, \quad (18)$$

if $J_c<J_T$. The time dependence of J from its minimum value during an oscillation period can be obtained by integrating Eq. (13) along the dashed line (nullcline) of Fig. 13. In the present case of $v_s=0$, Eq. (13) can be written as $[\Phi-(3J/2)\ln(r_a/r_c)]dJ/dt=\pi^2/32$, with the help of Eqs. (12) and (16). Upon integrating this equation,

$$J(t)=J_T\left(1-\sqrt{\left(1-\frac{J_{min}}{J_T}\right)^2-\frac{t}{t_T}}\right), \quad (19)$$

$$t_T=\frac{32\Phi^2}{3\pi^2\ln\left(\frac{r_a}{r_c}\right)}. \quad (20)$$

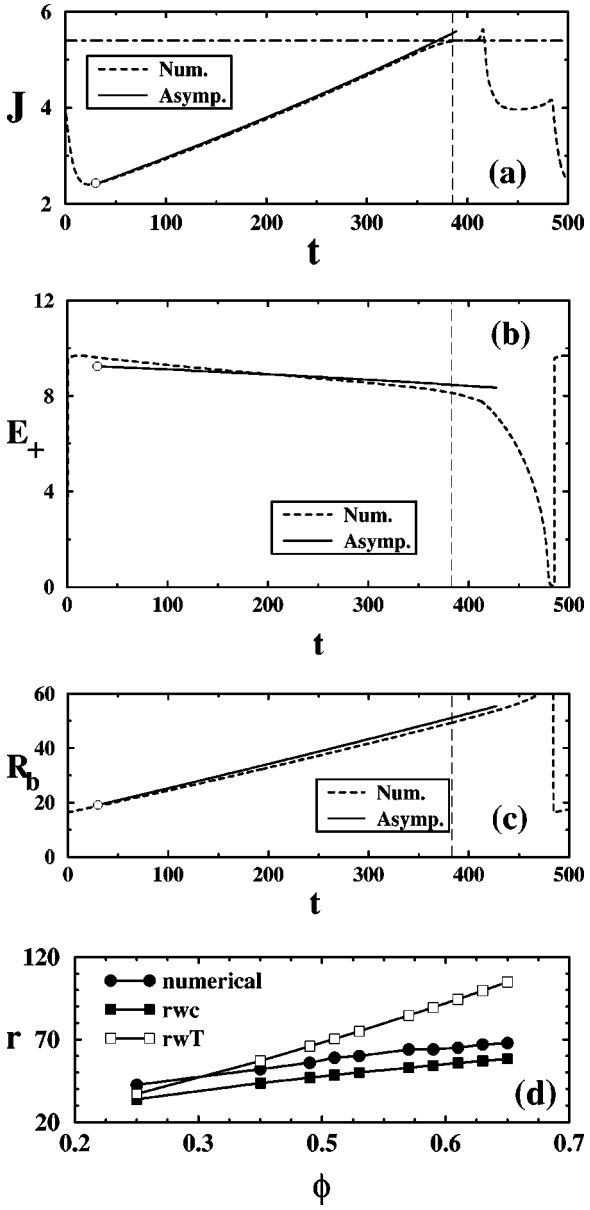

FIG. 14. Comparison of the asymptotic expressions for J, E_+, and R_b with the results of direct numerical solution starting with $J(t_0=30)=J_{min}\approx 2.4$. Parameter values are $r_c=10$, $r_a=90$, $\phi=0.6$, and $v_s=0$. (a) $J(t)$ (the horizontal line marks the critical current J_c). (b) $E_+(t)$. (c) $R_b(t)$. (d) Maximum radius as a function of bias. The numerically calculated maximum radius for the back of the pulse is compared to r_{wT} and r_{wc}. The difference of the latter with the numerically calculated R_b is the pulse width.

We have used, as initial condition, the minimum value of the current during one oscillation period, $J(0)=J_{min}$. A comparison of this approximation to a direct numerical solution of the whole problem is shown in Fig. 14.

For shorter samples such that $r_a<r_{wc}$ and large bias, the pulse reaches the anode before its maximal radius. Then the situation resembles the one-dimensional Gunn effect with a large voltage: a pulse reaches the anode before a new pulse is nucleated at the cathode [10]. If we relax the assumption $v_s=0$, we find that the pulse speed is faster according to Eq. (10). As in the case of $v_s=0$, there is also a maximum radius of the pulse (for large enough samples). In fact, the nullcline $dJ/dr_w=0$ has a turning point that can be found by solving

$$\frac{v_s}{C}z^3+\frac{3}{2}z^2-\Phi=0, \tag{21}$$

for $z>0$ as a function of Φ. Then J_T and r_{wT} are given by

$$z=E_+=\sqrt{2\left[\Phi-J_T\ln\left(\frac{r_a}{r_c}\right)\right]}, \tag{22}$$

$$r_{wT}=\frac{J_T z}{C}. \tag{23}$$

An approximate solution of the system of Eqs. (13) and (15) can be found as before. The maximum radius can be found by solving the simplified problem with the initial condition J_{min} and calculating the time that J needs to reach J_c. In general, the pulse reaches either its maximum radius or the anode (depending on L and ϕ) much earlier than in the case of $v_s=0$. This leads to small-amplitude current oscillations that may be rather irregular because J may be above J_c quite often, thereby producing new pulses near the cathode. See Fig. 12.

V. CONCLUSIONS

We have studied numerically the repeated generation and motion of axisymmetric pulses in a two-dimensional *n*-GaAs sample with a Corbino geometry. The field inside these pulses decreases as they advance and expand, so as to compensate their larger extension. Simultaneously, the current increases until a critical value is reached, and a new pulse is triggered at the central point contact. The current signal presents different patterns depending on the applied dc voltage bias. Just above the onset for self-oscillations, their amplitude is small and the pulse dies off shortly after it is generated. For larger voltages, self-oscillations have larger amplitude and pulses may or may not reach the outer sample boundary depending on the size thereof and bias. For sufficiently large samples, the pulse radius cannot surpass a maximum value given by an approximate analytical formula. Regions of aperiodic oscillations due to multipulse dynamics are interspersed with more regular periodic oscillations.

ACKNOWLEDGMENT

This work has been supported by the Spanish DGES through Grant No. PB98-0142-C04.

APPENDIX: OUTLINE OF THE NUMERICAL METHOD

We have used an efficient numerical scheme for partial differential equations with an integral constraint described and proved to converge in Ref. [11]. Radial derivatives are approximated by central differences, and a first-order implicit Euler method is used to integrate the resulting differential equations in time. This procedure results in having to solve a system of $(N+1)$ linear equations for the values of

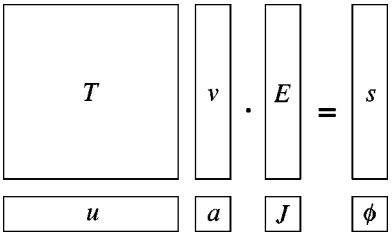

FIG. 15. Block matrix formulation of our numerical scheme to solve the equations for E and J.

the electric field and J at time t_{n+1} in terms of their previous values. The block matrix formulation of this system is shown in Fig. 15. There **T**, **u**, and **v** are a $N\times N$ tridiagonal matrix, a $1\times N$ row vector, and a $N\times 1$ column vector, respectively. Our system is, therefore, equivalent to

$$\mathbf{T}\cdot\mathbf{E}+J\mathbf{v}=\mathbf{s}, \tag{A1}$$

$$\mathbf{u}\cdot\mathbf{E}+Ja=\phi. \tag{A2}$$

This system can be efficiently solved by solving the following two systems with the same tridiagonal matrix:

$$\mathbf{T}\cdot\mathbf{y}=\mathbf{s}, \tag{A3}$$

$$\mathbf{T}\cdot\mathbf{z}=\mathbf{v}. \tag{A4}$$

In terms of **y** and **z**, we obtain

$$\mathbf{E}=\mathbf{y}-J\mathbf{z}, \tag{A5}$$

$$J=\frac{\mathbf{u}\cdot\mathbf{y}-\phi}{\mathbf{u}\cdot\mathbf{z}-a}. \tag{A6}$$

Thus we proceed by first obtaining the LU factorization of **T** and second carrying out two back substitution processes to solve Eqs. (A3) and (A4). Then Eqs. (A6) and (A5) yield J and **E**, respectively.

[1] J.D. Murray, *Mathematical Biology*, 2nd ed. (Springer, Berlin, 1993).
[2] J.P. Keener and J. Sneyd, *Mathematical Physiology* (Springer, New York, 1998).
[3] Y. Kuramoto, *Chemical Oscillations, Waves, and Turbulence* (Springer, Berlin, 1984).
[4] *Nonlinear Dynamics and Pattern Formation in Semiconductors and Devices*, edited by F.-J. Niedernostheide, Springer Proceedings in Physics, Vol. 79 (Springer-Verlag, Berlin, 1995).
[5] B. Willing and J.C. Maan, Phys. Rev. B **49**, 13 995 (1994); B. Willing, Ph.D. thesis, University of Nijmegen, 1994.
[6] J.B. Gunn, Solid State Commun. **1**, 1 (1963).
[7] L.L. Bonilla, P.J. Hernando, M. Kindelan, and F. Piazza, Appl. Phys. Lett. **74**, 988 (1999).
[8] H. Kroemer, IEEE Trans. Electron Devices **ED-13**, 27 (1966).
[9] L.L. Bonilla, I.R. Cantalapiedra, G. Gomila, and J.M. Rubí, Phys. Rev. E **56**, 1500 (1997).
[10] F.J. Higuera and L.L. Bonilla, Physica D **57**, 161 (1992).
[11] A. Carpio, P.J. Hernando, and M. Kindelan, SIAM (Soc. Ind. Appl. Math.) J. Numer. Anal. **39**, 168 (2001).